Iraqi Journal of Physics, 2026
https://doi.org/10.30723/ijp.v24i1.1292

Vol.24, No.1, PP.76-84
P-ISSN: 2070-4003
E-ISSN: 2664-5548

Spectroscopic Analysis and Structural Characterization of Nickel Oxide Nanoparticles Prepared by Plasma Jet System

Tabarak F. Orabi[1*] and Kadhim A. Aadim[2]
[1]*Department of Physics, College of Science, University of Baghdad, Baghdad, Iraq*
[2]*Laser Institute for Postgraduate Studies, University of Baghdad*
[*]Corresponding author: tabarak.f@sc.uobaghdad.edu.iq

Abstract
This study explains how nickel oxide (NiO) nanoparticles are made using a plasma jet method at normal air pressure, using a direct current (DC) power supply set to a steady voltage of 13 kV. The properties of the plasma were studied using optical emission spectroscopy (OES) while changing the flow rates of argon gas to 0.25, 0.75, 1.75, and 2.25 L/min over a period of 6 minutes. NiO thin films were deposited on glass substrates and annealed at 270 °C. UV-visible spectroscopy confirmed the optical properties of the NiO nanoparticles, revealing a marked decrease in the energy band gap from 4 eV to 2.5 eV with an increase in gas flow rate. X-ray diffraction (XRD) analysis demonstrated that the films possessed a polycrystalline structure with a cubic crystal system. Atomic force microscopy (AFM) analysis showed that as the argon flow rates increased, the surface became rougher and the average size of the particles got smaller. This work shows that the plasma jet system is a new, fast, environmentally friendly, and scalable way to make high-purity NiO nanoparticles that have better optical properties. These results suggest promising applications of NiO nanoparticles in photovoltaic devices, solar cells, and other optoelectronic devices.

Article Info.

Keywords:
Drop Casting, OES, Plasma Jet, XRD, AFM.

Article history:
Received:May, 05, 2024
Revised: Oct. 19, 2024
Accepted: Oct. 21, 2024
Published:Mar.01,2026

1. Introduction
Plasma produced at atmospheric pressure is a source of spectral light emission, essential for spectroscopy performed by an argon gas flow [1]. Metal oxide nanostructures have become a focus of scientific research because their properties are greatly influenced by their size and shape. As these dimensions vary at the nanoscale, nanostructures exhibit unique behaviors and properties, such as variable electrical, optical, and chemical properties, making them highly valuable for a variety of applications. This size and shape dependence allows scientists to tailor these materials for specific uses, such as sensors, catalysts, and energy storage devices. Their high surface-to-volume ratio makes them promising candidates for various sensing applications, including gas, optical, humidity, and biosensors [2, 3].

Describes plasma jet electrolysis technology involving plasma electrodes operating in an atmospheric environment. In this process, the "plasma region" refers to the area around atoms where plasma is present, allowing atoms or molecules to interact with the charged particles (electrons and ions) within the plasma. These interactions can lead to changes in the atoms or molecules' behavior, often resulting in modifications to their chemical or physical properties.

The cathode plays a central role in fabricating nickel oxide (NiO) nanoparticles, while the anode is made from a strip of nickel immersed in a liquid-gaseous medium. Plasma is applied to initiate fluid transformations within this medium. This setup, known as the analytical media system, serves as a baseline or "blank" device for observing reactions [4, 5]. The plasma electrode is electrically connected to a system containing both electrons and ions, enabling electrolysis to occur. During this process, multiple reactions take place, one of which includes visible changes, such as the gradual color shift

in the gas over time, indicating ongoing chemical changes. NiO nanocrystals are generated by exposing nickel metal to argon plasma for 6 minutes.

Nanoparticles have recently attracted interest because of their uses and properties [6,7]. Plasma jet technology offers many advantages, including environmental friendliness, affordability, and the absence of expensive equipment requirements. Its potential applications include visible light stimulation of photo degradation of organic pollutants [8]. The optical properties of nano particles generated by plasma jets have also been investigated. The purpose of this study was to validate the use of plasma jets in determining the crystalline structure and purity of nickel phases in nanoparticles produced under atmospheric pressure [9-11]. Plasma jets, consisting of pure nickel atoms surrounding the plasma, were analyzed to confirm their structural properties. The arrangement and structural characteristics of the nanoparticles were investigated using X-ray diffraction (XRD) technology, which revealed rhombic crystal structures [12, 13]. In addition, atomic force microscope (AFM) was used to examine the produced nanoparticles [14]. Plasma produced at atmospheric pressure is a source of spectral light emission, which is essential for spectroscopy performed by an argon gas flow [15]. This approach is used in multiple fields, where photoemission is induced by argon gas flow using cathode and anode electrodes, at a constant voltage of 13 kV.

Plasma properties and interactions are affected by factors such as temperature, electron density, Debye length, and plasma frequency [16, 17]. Optical spectroscopy is used to diagnose plasma under atmospheric pressure conditions, and emission spectroscopy is a powerful diagnostic tool used to examine the radiation emitted by plasma to ascertain quantitative and qualitative plasma characteristics. Such as electron temperature (T_e) using a Boltzmann diagram [18]. This research looks at the properties of nickel oxide (NiO) made in tiny sizes using plasma jet technology, by examining its crystal structure, particle size, how the particles are spread out, and the physical properties that come from how it was made. The research also aims to evaluate the effect of plasma jet technology on the quality and homogeneity of the material's nanostructure, compared to traditional preparation methods, which contributes to a more profound understanding of its potential use in industrial, electronic, and energy applications.

2. Experiment Work

NiO nanoparticles were synthesized using an atmospheric plasma jet, as illustrated in Fig. 1, which shows the experimental setup for the plasma jet and optical emission spectroscopy (OES) technique. The process used a stainless-steel tube with a 1.0 mm internal diameter and 3 cm length as the cathode, while a nickel strip (1 cm wide and 6 cm long) served as the anode, positioned 3 cm from the cathode. This strip was immersed in a non-ionic liquid and exposed to the plasma jet for a duration of 6 minutes at various gas flow rates. Argon gas was supplied as the discharge medium at a 5 L/min flow rate [19], with a 10 ml glass beaker containing 6 ml of nonionic water. A constant DC voltage of 13 kV was applied to initiate the discharge. During the initial stage, nickel oxide was generated in the form of a nano-solution, which was subsequently converted into a nano-membrane through drop-casting at a rate of 10 drops over 3 minutes onto a glass slide, followed by drying in an oven at 270°C.

3. Results and Discussion

3.1. Plasma Spectrum

Using a photoemission spectrometer (S3000-UV-NIR), nickel oxide plasma spectrum for different gas flow rates (0.25L/min-2.25L/min) was obtained as shown in Fig. 2. The spectrum displays emission lines of both atoms and ions, indicating the presence of a variety of elements. The spectral emission of the NiO target is depicted

utilizing the plasma jet technique. When the gas flow rate increased [20] the emission lines increased, and this led to an increase in the number of excited electrons. It has been determining the electron temperature, electron density, and plasma frequency shown in Table 1, the light emission spectrum of NiO and plasma generation using plasma jet technology were studied at a constant voltage difference of 13 kV, and for different argon gas flow rates (0.25, 0.75, 1.75 and 2.25 L/min); the gas was flowing for 6 minutes for each rate. The plasma spectrum of argon gas was obtained at the wavelength (550-1000) nm, as well as with data of the spectrum of NiO recorded at the wavelength (200-400) nm. The recorded data was analyzed and matched with data from the National Institute of Standards and Technology (NIST) [21].

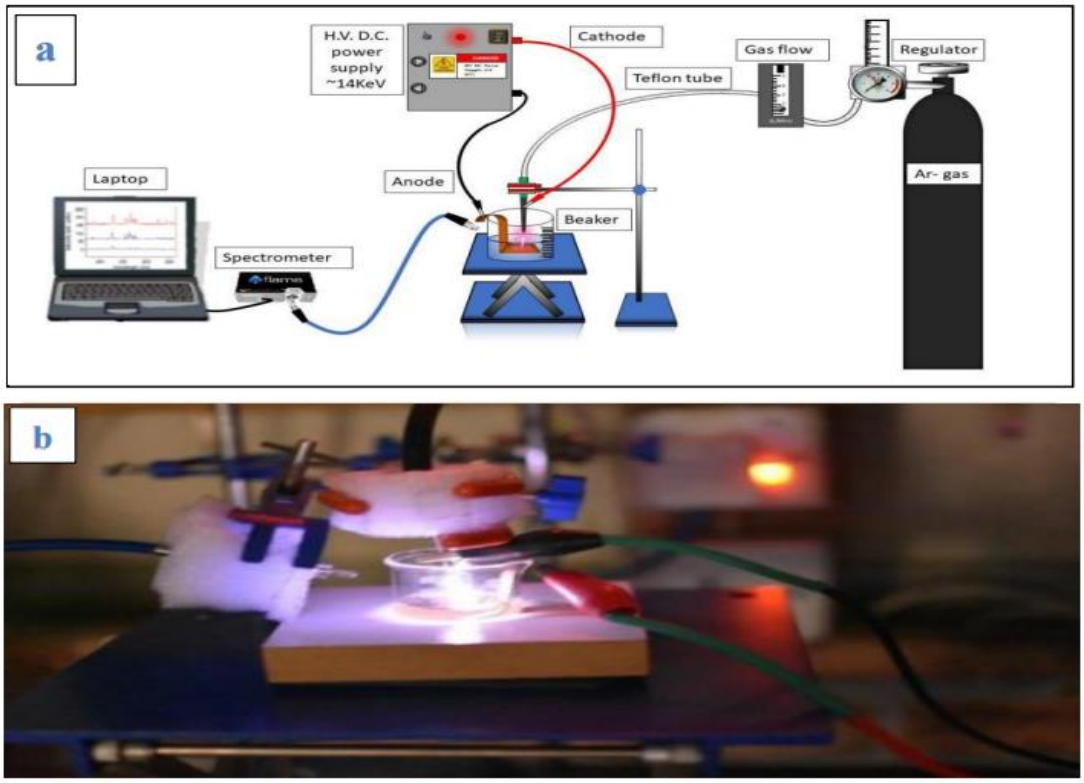

Figure 1:. a) Schematic diagram of a DC plasma jet with accompanying optical emission spectroscopic diagnostics. b) During the OES diagnostics, the configuration of the plasma jet system [1].

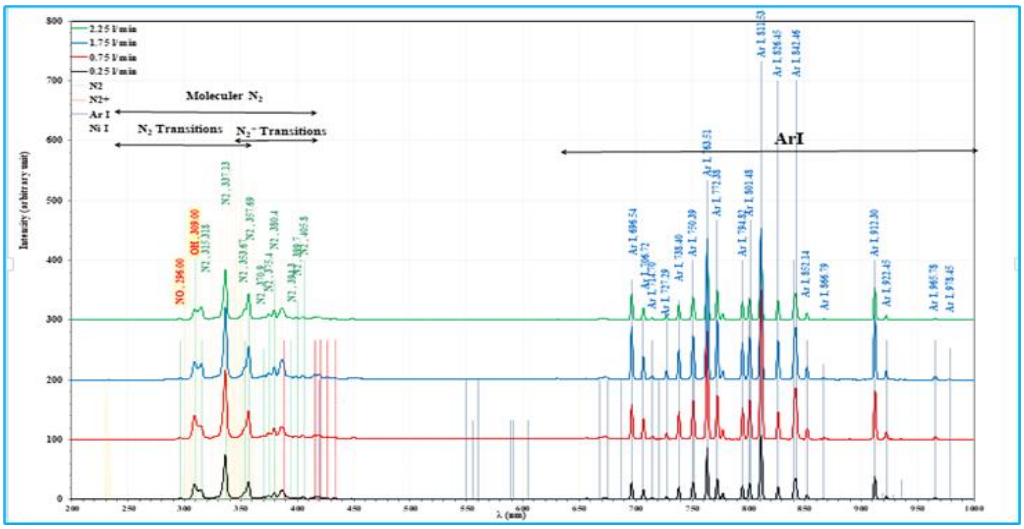

Figure 2: Optical emission spectroscopy was utilized to study NiO plasma's intensity and wavelength characteristics.

Table 1: Nickel plasma parameters at different argon gas flow rates (0.25 to 2.25 L/min).

Flow (L/min)	T_e (eV)	FWHM (nm)	$n_e x10^{17}$ (cm^{-3})	f_p $x10^{12}$ (Hz)	$\lambda_D x10^6$ (cm)	N_d
0.25	0.965	1.600	10.811	9.337	7.018	1565
0.75	0.951	1.800	12.162	9.903	6.570	1445
1.75	0.855	2.000	13.514	10.439	5.909	1168
2.25	0.837	2.100	14.189	10.697	5.705	1104

NiO thin films were prepared (nano-solution prepared using plasma jet technology) using drop casting show in Fig.3, in an electric furnace at a temperature of 270 °C and at different flow rates to perform optical examinations to determine the crystalline structure of the deposited film layer using XRD and to determine crystal size with the AFM.

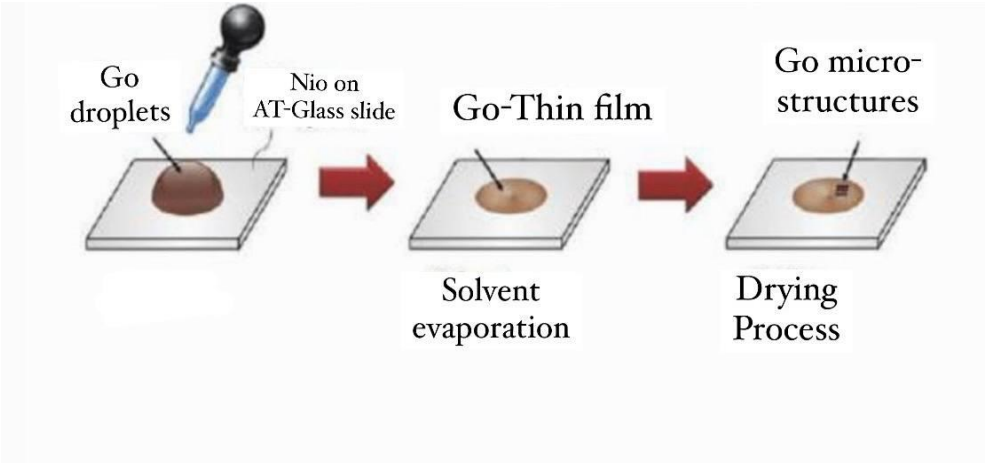

Figure 3: Drop-casting technique on a glass slide in an electric oven at 270 °C.

The crystal structure and phase purity of NiO nanoparticles synthesized using atmospheric plasma jets (APJs) were confirmed through XRD analysis. The XRD pattern, recorded within an angle range of 2θ from 20 to 80 degree for NiO nanoparticles, is illustrated in Fig. 4. In the XRD pattern of the nanoparticles, diffraction peaks appeared at 37.3305°, 43.25° and 62.7542°, corresponding to the NiO cubic structure and indexed to the Miller indices (111), (200), and (220), respectively [22]. This cubic structure aligns with previous research findings [23].

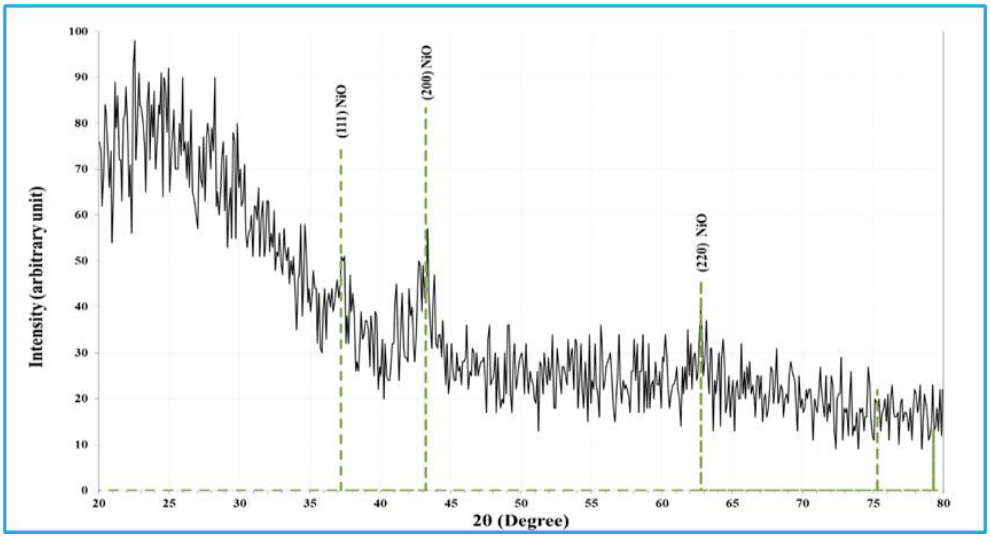

Figure 4: XRD pattern of NiO Core/Shell NPs synthesis by plasma jet technology.

The Debye-Scherer Eq. (1) [24] was employed to determine the nanoparticle crystallite sizes of the NiO nanoparticles.

$$D(\text{Å}) = \frac{K\lambda}{\beta \cos\theta} \quad (1)$$

In this context, D represents the crystallite size, K denotes Scherer's constant (K=0.9), λ signifies the X-ray wavelength (2.4069, 2.0935, and 1.4794 Å), and β stands for the Full Width at Half Maximum (FWHM) in radians of the peaks measured at the θ diffracting angle relative to the Bragg's angle position. The NiO and nanoparticles (NPs) average crystalline sizes were 11.6 nm and 10.0 nm, respectively. Consequently, the total average crystallite size is calculated as 10.6 nm, as shown in Table 2. The attractive physical forces acting between the nanoparticles bound them together or agglomerated them.

Table 2: XRD Parameters for NiO films at (0.25, 0.75, 1.75, and 2.25).

2θ (Deg.)	FWHM (Deg.)	d_{hkl} Exp.(Å)	hkl	Phase	D (nm)	Average D(nm)
37.3305	0.7203	2.4069	(111)	Cub-NIO	11.6	
43.1780	0.8475	2.0935	(200)	Cub-NIO	10.1	10.6
62.7542	0.9322	1.4794	(220)	Cub-NIO	10.0	

3. 3. Atomic Force Microscopy (AFM)

NiO thin films were made by dropping a liquid solution created using a plasma jet in an electric furnace at 270 degrees. The nanofilms prepared using the described method were analyzed using atomic AFM [25]. Fig.5 presents 3D topographic views obtained from the AFM and an image of the thin film. This analysis provides detailed surface morphology and structural information about the nanofilms. The AFM image illustrates that annealing significantly influences the surface morphology. The AFM parameters for the sample in Fig. 5 are: RMS (Root Mean Square) of 3.296 nm, average roughness of 2.572 nm, and an average diameter of 41.54 nm.

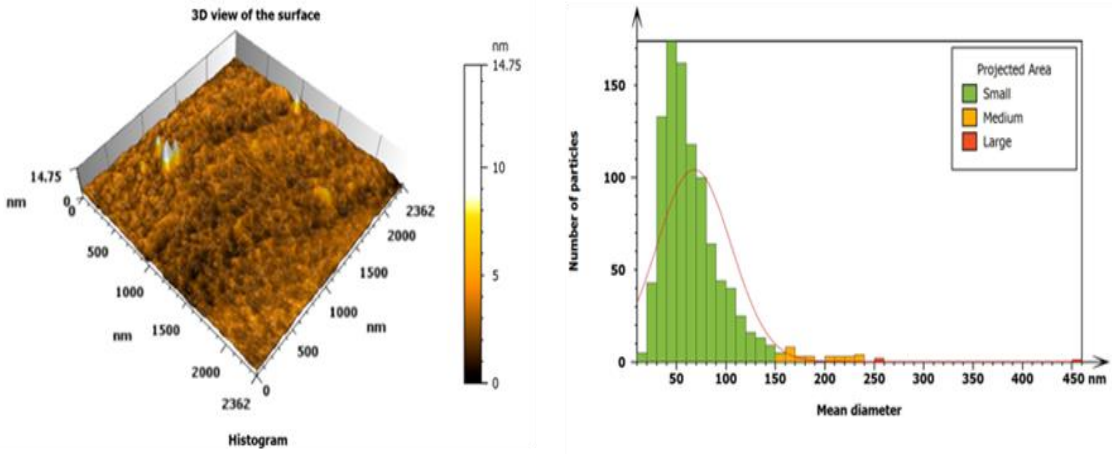

Figure 5: 3D AFM and grain accumulation distribution of NiO thin films prepared by Drop casting technology at a temperature of 270 degrees Celsius for an argon gas flow rate of 0.75L/min.

3. 4. Optical Properties

The UV-Vis spectroscopy technique was employed to characterize the optical absorption properties of NiO nanoparticles generated via the atmospheric plasma jets (APJs) method. This optical method enabled a close look at how the nanoparticles absorb light in the UV and visible ranges, providing important information about their physical properties, such as absorbance and band gap energy. A UV-Vis spectrophotometer operates by measuring the absorption of light by the sample. The band gap, a crucial optical parameter, was determined through plotting experimental absorbance data, a common technique for measuring the optical band gap of nanoparticles. The band gap was directly measured from the cutoff by applying Planck's law [26], as depicted in Eq. (2):

$$E_g = \frac{hc}{\lambda} = \frac{1240}{\lambda} \quad \textbf{(2)}$$

where E_g is the optical energy gap, h is Planck's constant (6.626×10^{-34} Js), c is the velocity of light (3×10^{8} m/s), and λ is the cut-off wavelength corresponding to the optical band gap. λ was determined graphically from linear region extrapolation in Fig.6, which shows the UV–Vis absorption spectra of nickel oxide nanoparticles as a function of wavelength at room temperature. The nickel oxide core nanoparticles were investigated using UV–Vis absorption measurements obtained from nanoparticles synthesized by atmospheric plasma jetting.

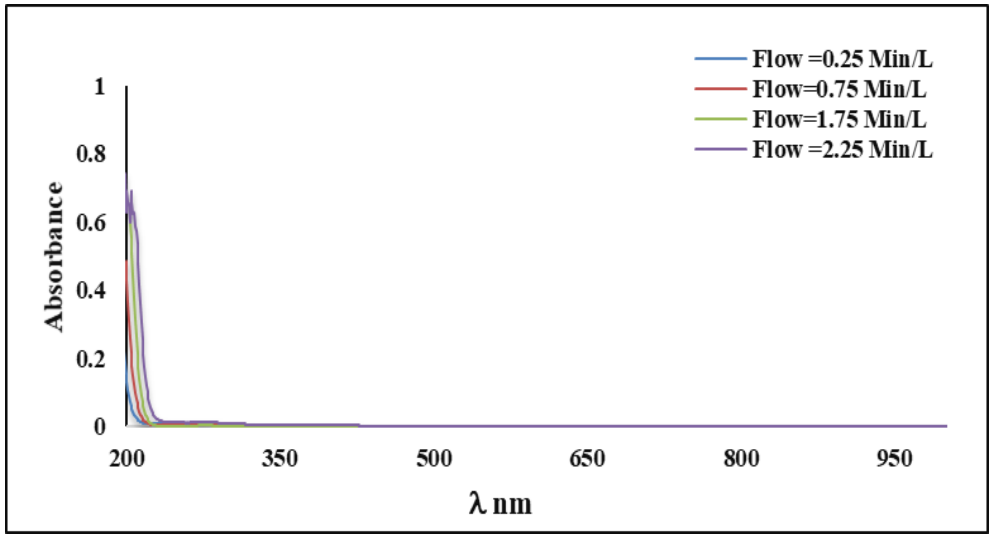

Figure 6: Optical absorption Spectrum of nickel oxide nanoparticles.

Broad absorption peaks were observed for NPs assessed within the wavelength range of 200 to 1100 nm. By utilizing the absorbance spectra, the absorption coefficients of the NiO nanoparticles were determined graphically show in Fig.7, through the application of Tauc's relationship for direct transition [27], represented by Eq. (3)

$$(\alpha h\nu)^r = A(h\nu - E_g) \quad \textbf{(3)}$$

where α is the absorption coefficient, υ is the incident photon frequency, A is a constant equal to 0.9, and r is a value that depends on the nature of the transition type (r = 2) for the allowed direct transition.

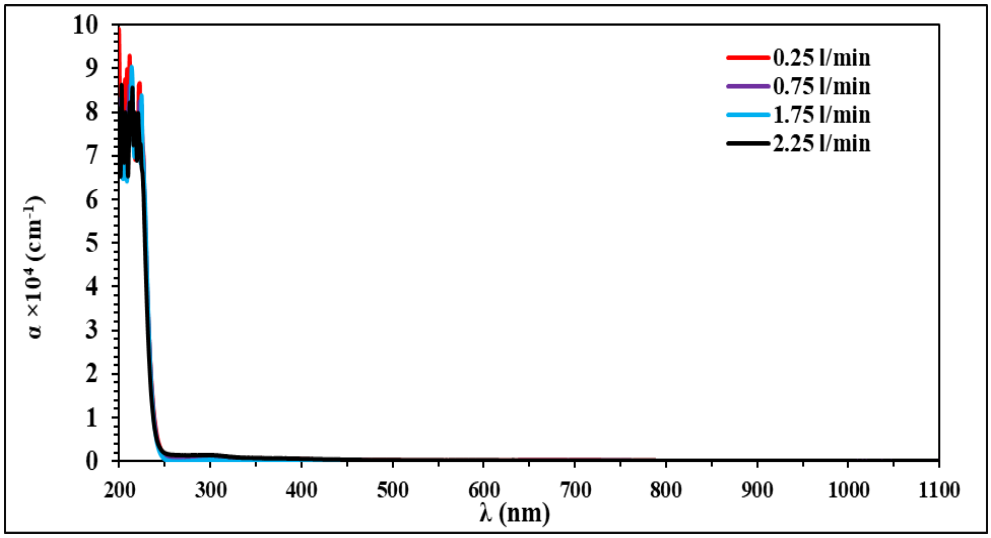

Figure 7: the variation of absorption coefficient with wavelength for NiO nanoparticles at different Argon gas flow rates.

The spectral analysis indicated that the absorption coefficient of all nickel oxide nanoparticles decreases to values of 8.8 and 8.6 at flow rates of 0.75 and 2.25, respectively, as the wavelength increases from 250 to 1100 nm. Conversely, the increase in the absorption coefficient suggests a reduction in reflection and transmission. Additionally, it was observed that the absorption peaks shift to higher wavelengths (lower photon energy) as the gas flow rate increases, represented by the black lines in all figures.

A common method for determining the band gap involves plotting a graph of photon energy (hυ) in eV versus $(\alpha h\upsilon)^2$ and extrapolating the straight line to its intersection with the axis, as shown in Fig. 8. This figure illustrates that increasing the argon gas flow rate from 0.25 to 2.25 L/min led to a decrease in the energy gap, reducing it from approximately 4 eV to about 2.5 eV. For NiO nanoparticles, the energy gap values align well with the findings reported by Aadim [27].

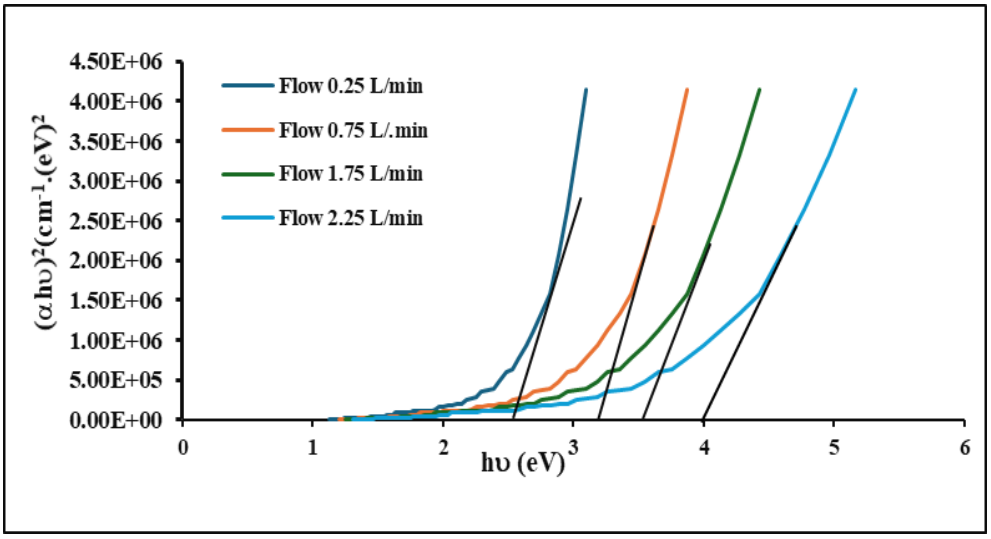

Figure 8: Energy gap Optical for liquid NIO NPs.

4. Conclusions

This study monitored the formation of nickel oxide nanoparticles using a plasma jet technique. By changing the flow rates of argon gas, we found specific absorption peaks, which showed that nickel oxide was successfully made. The nanoparticles

demonstrated excellent optical absorption properties, underscoring their potential for visible light applications, particularly in photovoltaics. This synthesis method distinguishes itself from others due to its simplicity, speed, cost-effectiveness, and environmental sustainability, making it an attractive option for nanoparticle production. Structural analysis, confirmed by XRD, showed that the nanoparticles were highly pure and fully crystalline. AFM observations showed that when the argon flow rate went up, the average size of the particles got smaller, but the surface became rougher, indicating a change in the shape of the nanoparticles.

Conflict of Interest

The authors declare that they have no conflict of interest.

References

1. I. K. Abbas and Kadhim A. Aadim, Iraqi J. Sci. **64**, 2271 (2023). https://doi.org/10.24996/ijs.2023.64.5.15.
2. J. A. Castillo and I. V. Blanco, Revista Tecnología En Marcha. **29**, 47 (2016). http://dx.doi.org/10.18845/tm.v29i6.2901.
3. M. H. Ahmed, H. R. Humud, Iraqi J. Sci. **23**, 128 (2025). https://doi.org/10.30723/ijp.v23i3.1305
4. H. J. Imran, K. A. Hubeatir, and K. A. Aadim, Sci. Rep. **13**, 5441 (2023). https://doi.org/10.1038/s41598-023-32330-z.
5. P. Lamichhane, T. R. Acharya, N. Kaushik, L. N. Nguyen, J. S. Lim, V. Hessel, N. K. Kaushik, and E. H. Choi, J. Envir. Chem. Eng. **10**, 107782 (2022). https://doi.org/10.1016/j.jece.2022.107782.
6. R. Zaplotnik, G. Primc, and A. Vesel, Appl. Sci. **11**, 2275 (2021). https://doi.org/10.3390/app11052275.
7. H. B. Baniya, R. Shrestha, R. P. Guragain, M. B. Kshetri, B. P. Pandey, and D. P. Subedi, Int. J. Poly. Sci. **2020**, 9247642 (2020). https://doi.org/10.1155/2020/9247642.
8. D. Hope, T. Cox, and V. Deshmukh, Vacuum **37**, 275 (1987). https://doi.org/10.1016/0042-207X(87)90008-X.
9. I. Adamovich, S. D. Baalrud, A. Bogaerts, P. J. Bruggeman, M. Cappelli, V. Colombo, U. Czarnetzki, U. Ebert, J. G. Eden, P. Favia, D. B. Graves, S. Hamaguchi, G. Hieftje, M. Hori, I. D. Kaganovich, U. Kortshagen, M. J. Kushner, N. J. Mason, S. Mazouffre, S. M. Thagard, H. R. Metelmann, A. Mizuno, E. Moreau, A. B. Murphy, B. A. Niemira, G. S. Oehrlein, Z. L. Petrovic, L. C. Pitchford, Y. K. Pu, S. Rauf, O. Sakai, S. Samukawa, S. Starikovskaia, J. Tennyson, K. Terashima, M. M. Turner, M. C. M. Van De Sanden, and A. Vardelle, J. Phys. D: Appl. Phys. **50**, 323001 (2017). https://doi.org/10.1088/1361-6463/aa76f5.
10. 10. S. J. Kadhem, Iraqi J. Sci. **19**, 44 (2021). https://doi.org/10.30723/ijp.v19i48.593.
11. A. Hyde and O. Batishchev, Rev. Sci. Instrum. **91**, 063502 (2020). https://doi.org/10.1063/1.5141486.
12. R. Shrestha, D. Subedi, J. Gurung, and C. Wong, Sains Malaysiana **45**, 1689 (2016).
13. F. Wu, J. Li, Y. Xian, X. Tan, and X. Lu, Plas. Proce. Poly. **18**, 2100033 (2021). https://doi.org/10.1002/ppap.202100033.
14. J. Y. Pae, R. Medwal, J. V. Vas, M. V. Matham, and R. S. Rawat, J. Vac. Sci. Tech. B **37**, 041201 (2019). https://doi.org/10.1116/1.5093241.
15. M. Fikry, W. Tawfik, and M. Omar, J Russian Laser Res. **41**, 484 (2020). https://doi.org/10.1007/s10946-020-09901-w.
16. A. M. El Sherbini and A. A. S. Al Aamer, World J. Nano Sci. Eng. **2**, 206 (2012). https://doi.org/10.4236/wjnse.2012.24028.
17. B. M. Smirnov, *Physics of Ionized Gases* (Canada, John Wiley & Sons, 2001).
18. S. Chandra, *Textbook of Plasma Physics* (India, CBS Publishers & Distributors Pvt. Ltd, 2017).
19. B. Subramanian, M. Mohamed Ibrahim, V. Senthilkumar, K.R. Murali, VS. Vidhya, C. Sanjeeviraja, M. Jayachandran, Physica B**, 403**, 4104 (2008) https://doi.org/10.1016/j.physb.2008.08.014.
20. A. Bouhank, Y. Bellal and H. Serra, J. Chem. Chem. Eng. **12,** 116(2018). https://doi.org/10.17265/1934-7375/2018.03.005.
21. J. H. Adawiy, R. Al- Anbari, H.M. Sami, M.J.Haider, Energy Procedia **15**,1328(2019). https://doi.org/10.1016/j.egypro.2018.11.298.
22. M. Obaida, Ahlam M. Fathi, I. Moussa, H. H. Afify, Journal of Materials Research, **37**, 2282 (2022) https://doi.org/10.1557/s43578-022-00627-w.
23. N. Mebrouki, S. B. Hamida, L. Benmebrouk, R. Gheriani, L. Zenkhri, Asian Journal of Research in Chemistry. **15**,159(2022). https://doi.org/10.52711/0974-4150.2022.00026.

24. L.-Y. Xie, D.-Q. Xiao, J.-X. Pei, J. Huo, X. Wu, W.-J. Liu and S.-J. Ding, Mater. Res. Express, **7**, 046401(2020). https://doi.org/10.1088/2053-1591/ab82c9.
25. A. H. Hammad, M. Sh. Abdel-Wahab, S. Vattamkandathil and A. R. Ansari, Coatings, **9**, 615(2019) https://doi.org/10.3390/coatings9100615.
26. R. A. Ismail, S. Ghafori, G. A. Kadhim, Appl Nanosci, **3**, 509(2013) https://doi.org/10.1007/s13204-012-0152-2.
27. P. Salunkhe, M. Ali, and D. Kekuda, Mater. Res. Express, **7**, 016427(2020) https://doi.org/10.1088/2053-1591/ab69c5.

التحليل الطيفي والتوصيف الهيكلي لجسيمات اوكسيد النيكل النانوية المحضرة بواسطة نظام بلازما النفث

تبارك فاضل عريبي[1] وكاظم عبد الواحد عادم[2]
[1]قسم الفيزياء، كلية العلوم، جامعة بغداد، بغداد، العراق
[2]معهد الليزر للدراسات العليا، جامعة بغداد، بغداد، العراق

الخلاصة

تتناول هذه الورقة تفاصيل تصنيع جسيمات اوكسيد النيكل النانوية باستخدام تقنية البلازما النفاثة تحت الضغط الجوي. تم إجراء التحليل الطيفي للانبعاث البصري(OES) بمعدلات تدفق غاز الأرجون متفاوتة (0.25، 0.75، 1.75و2.25) لمدة 6 دقائق عند جهد ثابت قدره 13 كيلو فولت. تم تصنيع أغشية رقيقة من الجسيمات النانوية السائلة عن طريق ترسيب المسبوكات على شرائح زجاجية باستخدام فرن كهربائي عند درجة حرارة 270 درجة مئوية، وتم تحليل خصائصها البصرية عن طريق الفحص الطيفي على وجه التحديد الأشعة فوق البنفسجية لتأكيد توصيف الجسيمات النانوية. NiO تشير النتائج إلى أن فجوة الطاقة تقل من4 الكترون فولت إلى 2.5 الكترون فولت مع زيادة معدل تدفق الغاز. أظهر تحليل حيود الأشعة السينية (XRD) أن الأغشية تمتلك بنية متعددة البلورات بنظام بلوري مكعب. أظهر تحليل المجهر الذري للقوة (AFM) زيادة في خشونة الجذر التربيعي المتوسط (RMS) وانخفاضًا في متوسط قطر الجسيمات كلما زاد معدل تدفق غاز الأرجون. يوضح هذا العمل حداثة نظام نفث البلازما كطريقة سريعة وصديقة للبيئة وقابلة للتطوير لتوليف جسيمات نانوية عالية النقاء من أكسيد النيكل، والتي تتميز بخصائص بصرية محسنة. تشير هذه النتائج إلى تطبيقات واعدة لجسيمات أكسيد النيكل النانوية في الأنظمة الكهروضوئية والخلايا الشمسية والأجهزة البصرية الإلكترونية الأخرى.

الكلمات المفتاحية: إسقاط الصب، طيف الانبعاث البصري، نفث البلازما، طيف الاشعة السينية، مجهز القوة الذرية.